EXPERIMENTAL AND NUMERICAL INVESTIGATION ON THE FAILURE MODES OF THICK COMPOSITE LAMINATES

Airoldi A.* , Sala G.* , Pasqualini F.*
***Aerospace Engineering Department, Politecnico di Milano, Italy**

Keywords: *composites, interlaminar stress, cohesive elements*

Abstract

The paper presents the results of experiments designed to point out the role of interlaminar stress on the bending failure of thick composite laminates with geometrical variations and plies discontinuities. A numerical approach is developed using the HKS/Abaqus Explicit code in order to predict interlaminar damage nucleation and propagation in thick laminates with explicit finite element analyses. Non-linear constitutive laws are applied to model inelastic mechanisms in the interlaminar layers as well as in the plies of the laminate. The numerical-experimental correlations show that the proposed numerical technique can model complex three dimensional stress states in the laminate as well as the damage development and its effect on failure modes of the laminates.

1 Introduction

The considerable in-plane stiffness and strength properties of composite plies may be exploited to efficiently design thick parts of the primary structures of aircraft. These structural parts are designed to obtain high stiffness and to carry high loads without experiencing failures due to the stress states acting in the plane of the composite plies. However, in such conditions, the out-of-plane stress components may reach critical levels and induce the nucleation of interlaminar damage so to influence the strength of the thick composite part.

Complex three dimensional stress states in a thick composite laminate can not be analyzed by means of finite element schemes using layered shell elements. Moreover, once an interlaminar crack is nucleated, its propagation and the possible failure of the laminate depend on the toughness of the interlaminar layers and on the energy available to propagate the crack.

Accordingly, the prediction of the ultimate load carrying capability of a laminate, taking into account the effects of interlaminar failures, requires highly refined finite element schemes and the capability to model the strength as well as the toughness of the interlaminar layers.

A promising approach to accomplish such objectives is to use interface elements in order to represent the interlaminar layers between the composite plies [1,2]. These elements, also referred to as cohesive elements, have been already applied to model interlaminar failure process in composites, considering pre-cracked specimens, the debonding of stiffeners parts from composite structures as well as impacts on composite skins [3,4,5,6,7,8,9,10,11]. The application of these techniques to model the possible development of interlaminar fractures in an undamaged thick laminate implies several difficulties, particularly when the locations of possible development of interlaminar fractures can not be easily a-priori predicted.

The objective of the paper is to investigate the possible effects of interlaminar damage on the response of thick laminates in bending and to propose a numerical approach to model in-plane and out-of-plane inelastic mechanisms in the composite. The experimental results will be presented at first and the basic aspects of the modeling technique will be outlined. Finally, the models and the numerical analyses of the experiments carried out with the HKS/Abaqus Explicit code will be described correlating the results with the experimental data.

2 Bending experiments on thick fabric composite laminate

2.1 Objective of the experiments and experimental apparatus

The experimental activities presented in this work were designed to compare the responses and the failure modes of a laminate in bending conditions with progressively increasing levels of the out-of-plane stress components.

To accomplish such objective, three different tests were performed on 300 mm long and 36 mm wide thick composite elements, made of woven fabric plies, varying the geometry, the lay-up sequence and the load conditions of the laminate. The first specimen, shown in Fig. 1-A, was a plane specimen with a cross-ply lay-up $([0][90])_{7S}$. The second and the third specimen, shown in Fig. 1-B and 1-C, respectively, presented a tapered zone with a transition from a lay-up having fibers in the 0°, 90° an +/-45° direction to the $([0][90])_{7S}$ cross-ply lay-up. Figure 2 shows a detail of the transition zone. The tapered specimens were designed to perform a three-points (Fig. 1-B) and a four-points (Fig. 1-C) bending test.

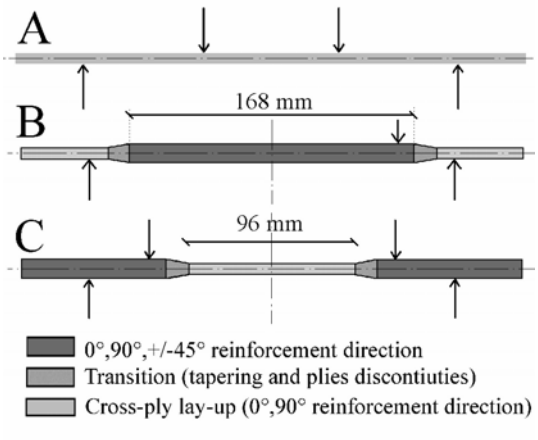

Fig. 1. Thick laminate specimens

The specimen were manufactured with a vacuum-bag process using a plane weave fabric pre-preg, with T800 carbon fibers and an Hexcel 1947 epoxy resin. The thickness of the obtained specimens varied in the range 6.12÷6.30 mm and 11.30÷11.55 mm in the thin and in thick parts of the laminates, respectively.

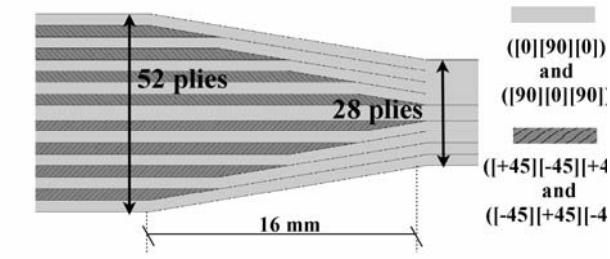

Fig. 2. Detail of the tapered specimens

The experimental apparatus consisted of a steel rig fixed to an MTS Alliance RF/200 static test system. Loads were applied by means of steel cylinders with a diameter of 30 mm.

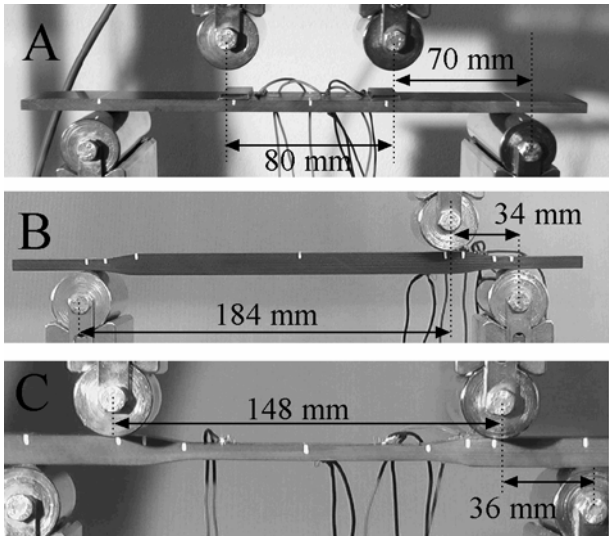

Fig. 3. Experimental set-ups

Figure 3 presents the test set-up of the three experiments. In order to prevent failures under the point of load applications, two elastomeric pads were located under the inner cylinders in the reference test (Fig. 3-A). The compression of the pads was measured by means of on optical transducer. Cross-head displacements, load levels as well as strain measures were acquired in the tests that were performed at 1.0 mm/min cross head speed and recorded by a digital camera.

To obtain a characterization of the material properties in tension and shear, two tensile tests were also performed on $([0][90])_{2S}$ and on $([+45][-45])_{2S}$ laminates according to ASTM D3039/D 3039M and ASTM D 3518/D 3518M, respectively.

2.2 Experimental results

Figure 4 reports the experimental force vs. cylinder displacement curves relevant to all the performed bending tests. For each test, three valid experiments were performed. The force vs. displacement test data were interpolated at given displacement levels to obtain the mean force vs. displacement curves. Figure 4 also shows that the original test data present a low scattering level with respect to the obtained mean curves, with the exception of a single three point bending test.

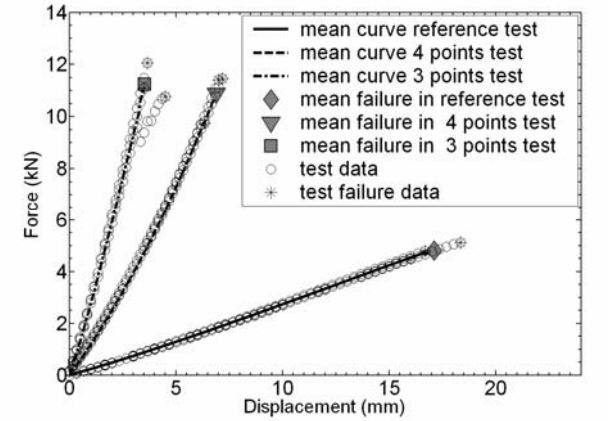

Fig. 4. Experimental bending responses

In the reference test, all the laminates failed by compressive failure of the upper plies in the gauge length of the specimens (Fig. 5). The experimental strains measured on the upper and lower surface of these specimens also indicate that the compressive elastic modulus is lower than the tensile one and allowed to set a mean strain at compressive failure, ε_c^U , of 11130 με.

In the four-points bending tests the development of an interlaminar damage was observed before the failure of the specimens, in all the performed experiments.

Fig. 5. Failure mode in the reference test

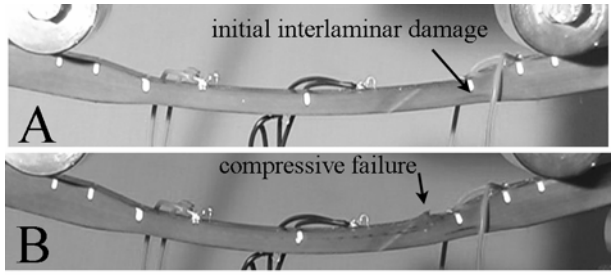

Fig. 6. Failure in the four-points bending tests

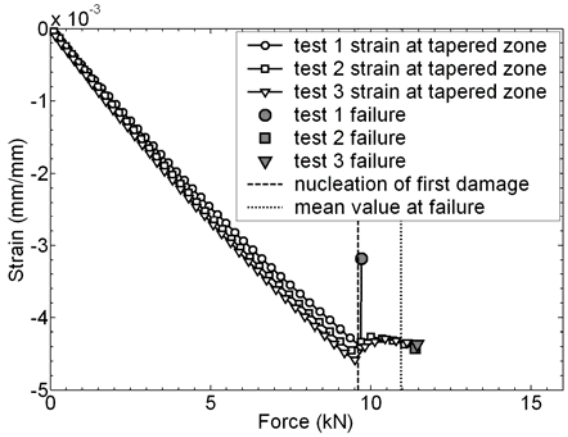

Fig. 7. Strain at the tapered zone in the four-points bending tests

The typical behaviour is shown in Fig. 6: a crack onset in the lower half of the tapered zone (Fig. 6-A), before the compressive failure of upper plies at the end of the tapered zone (Fig. 6-B). The strains acquired by strain gauges located on the tapered parts confirmed, for all the tests, that the local strain in this zones deviated from a monotonic course before the ultimate load was reached, thus indicating that a damage developed in the transition zone (Fig. 7). The mean value of the load at the nucleation of the defect in the four-points bending test, F_{4p}^N, was 9.6 kN, while the mean ultimate load, F_{4p}^U, was 10.95 kN.

The failure of the specimens in the three-points bending tests occurred at a mean ultimate load F_{3p}^U of11.25 kN with the development of interlaminar cracks in the midplane of the specimens. Minor interlaminar damages also nucleated and propagated in the compressed half of the tapered part. The video and the typical force vs. displacement curves indicate that the ultimate load was indeed reached in correspondence of the unstable propagation of

the midplane cracks, when a sudden drop of load carrying capability was measured. Thereafter, the tests were prosecuted after the initial propagation of the cracks and subsequent phases of unstable propagation of the midplane fractures were observed, until the specimen was completely split in the zone shown in Fig. 8.

Fig. 8. Failure in the three-points bending tests

Globally, the failures obtained in the experiments were influenced by the presence of out-of-plane stress components at different degrees. Interlaminar damages were absent in the response of the reference test, while they nucleated, without propagation, in the four points bending test that exhibited a final failure still determined by the compressive in-plane strength of the plies. Finally, in the three points bending test, a failure mode exclusively due to the nucleation and propagation of interlaminar cracks was obtained.

3 Modeling approach

The presented experiments can be considered valuable test cases to assess a numerical approach to model the development of interlaminar damages in thick laminates.

Accordingly, finite element explicit analyses were performed with the aim to model the experimental overall responses, damage and failure modes.

To develop the numerical approach, a constitutive law originally proposed for zero-thickness cohesive elements [7] was modified and used within a different modeling technique capable to represent the cohesive fracture in the interlaminar layer between two sublaminates, modeled by means of shell elements. In-plane failures were represented exploiting a different constitutive model, developed in previous works [12,13,14]. The basic aspects of the modeling technique are hereby described and the constitutive laws briefly reviewed.

3.1 Basic aspects of the modeling technique

The developed modeling technique considers the laminate as an assembly of sublaminates, represented by means of shell elements. The decohesive process leading to the development of interlaminar cracks is represented basing on the relative displacements of the midplane of the sublaminates, at a distance *th* (Fig. 9).

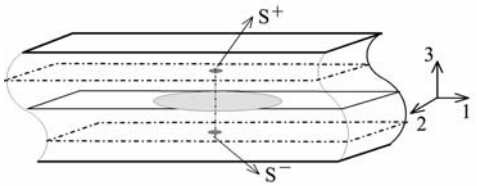

Fig. 9. Relative displacements between the middle plane of two sublaminates

The kinematic variables used to describe the fracture process in mode *I*, *II* and *III* are described by the vector $\{\Delta\}$ given in Eq. 1.

$$\begin{Bmatrix} \Delta_I \\ \Delta_{II} \\ \Delta_{III} \end{Bmatrix} = \begin{Bmatrix} S_1^+ - S_1^- \\ S_2^+ - S_2^- \\ S_3^+ - S_3^- \end{Bmatrix} \tag{1}$$

According to Fig. 9, the material volume between the midplanes of the sublaminates undergoes a strain state with out-of-plane components having mean values that can be represented by a vector $\{\varepsilon\}$. Within a small strain assumption, $\{\varepsilon\}$ can be immediately related to the relative displacement $\{\Delta\}$ as shown in Eq. 2.

$$\begin{aligned} \{\varepsilon\} &= \{\varepsilon_{33} \quad \gamma_{13} \quad \gamma_{23}\}^T \\ \{\varepsilon\} &= \{\Delta\}/th \end{aligned} \tag{2}$$

In the modeling technique, 8-nodes solid element with a reduced integration scheme were used to model the out-of-plane properties in the material volume between the mid-plane of sublaminates. These elements were used to connect the nodes of shells representing the

sublaminates (Fig. 10). The interlaminar decohesion process could be represented using the out-plane components of the strain state at the single integration point of the solids which were characterized to model the out-of-plane stiffness, strength and toughness of the composite. Accordingly, the out-of-plane elastic properties of the material, namely E_{33}, G_{13} and G_{23}, were attributed to the solid, while the in-plane stiffness of the composite was completely modeled by the layered shells, representing the sublaminates. The bending stiffness of a laminate modeled by such approach was proved to be equal to the one of a model made of layered shell elements [8].

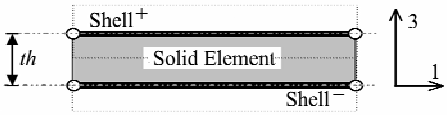

Fig. 10. Modelling technique

3.2 Modeling the strength and toughness of interlaminar layers

A simplification was introduced in the model of the interlaminar layer assuming that all the properties relevant to fractures developing in mode *II* and mode *III* was identical. This allowed to define two stress components acting in the interlaminar layer and driving fracture process determined by tensile (mode *I*) and shear stress (mode *II*) (Eq. 3).

$$\sigma_I = \begin{cases} 0 & if\ \sigma_{33} \le 0 \\ \sigma_{33} & if\ \sigma_{33} > 0 \end{cases} \qquad \sigma_{II} = \sqrt{\sigma_{13}^2 + \sigma_{23}^2} \tag{3}$$

The strength of the interlaminar layer was modeled using a quadratic criterion, as in [7,8], calibrated on the basis of the strength σ_I^0 and σ_{II}^0, referred to a decohesion process evolving in pure mode *I* and *II*, respectively (Eq. 4).

$$\sqrt{\left(\frac{\sigma_I}{\sigma_I^0}\right)^2 + \left(\frac{\sigma_{II}}{\sigma_{II}^0}\right)^2} = 1 \tag{4}$$

Under the assumptions introduced in [2], the interlaminar toughness do not depend on the crack length and can be modeled imposing that the work done by the interlaminar stress during decohesion process is equal to the critical energy release rates, G_{Ic} and G_{IIc}. Hence, Eq. 5 were obtained for process evolving according to the fracture modes *I* and *II*, after having defined the strain ε_I and ε_{II}, analogous to the stress σ_I and σ_{II} defined in Eq. 4.

$$\int_0^\infty \sigma_I d\Delta_I = th\int_0^\infty \sigma_I d\varepsilon_I = G_{Ic} \qquad \int_0^\infty \sigma_{II} d\Delta_{II} = th\int_0^\infty \sigma_{II} d\varepsilon_{II} = G_{IIc} \tag{5}$$

To fulfill Eq. 5, a continuum damage mechanics approach was adopted so to obtain a bi-linear constitutive response, characterized by final strains ε_I^F and ε_{II}^F, shown in Fig. 11. This response was completely determined by the strength and the toughness properties of the material.

Different formulation have been proposed to take into account the toughness in mixed mode fracture process. In this work, the model proposed in [7] was chosen and adapted to the material model attributed to the solid elements representing the interlaminar layer as described in [8]. Toughness in mixed mode is determined by a quadratic toughness criterion, expressed in Eq. 6.

$$\sqrt{\left(\frac{G_I}{G_{Ic}}\right)^2 + \left(\frac{G_{II}}{G_{IIc}}\right)^2} = 1 \tag{6}$$

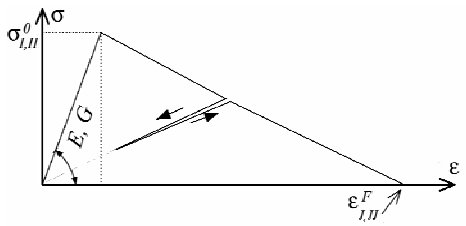

Fig. 11. Constitutive law of interlaminar layers

3.3 Modeling the in-plane behaviour of the plies

In order to model the in-plane response of sublaminates, a bi-phasic constitutive law developed in previous work [12,13,14] was adopted. The law models the response of a fabric ply by means of a decomposition into two idealized phases, the fiber and the matrix, as indicated in Eq. 7.

$$\begin{Bmatrix} \sigma_{11} \\ \sigma_{22} \\ \sigma_{12} \end{Bmatrix} = \left(\begin{bmatrix} E_1^f & 0 & 0 \\ 0 & E_2^f & 0 \\ 0 & 0 & 0 \end{bmatrix} + \left[E^m \right] \right) \begin{Bmatrix} \varepsilon_{11} \\ \varepsilon_{22} \\ \gamma_{12} \end{Bmatrix} \qquad (7)$$

A continuous damage mechanics approach is used to represent inelastic mechanisms due to brittle failures or progressive damages by means of different scalar damage variables, which are attributed to the different phases. The detail of the model and of the relevant calibration procedures can be found in [12,13,14].

4 Numerical models of the bending tests

Both the in-plane bi-phasic law as well as the constitutive law to model interlaminar layers were implemented in a user subroutine linked to the HKS/Abaqus Explicit code. The material models were thus made available to characterize the elements in the finite element schemes of the previously described specimens in order to perform explicit analyses of the bending tests.

4.1 Finite element schemes

The finite element schemes of the specimens were developed using first order shell element (type *S4R* [15]) to represent composite sublaminates which were connected by means of first order solid elements (type *C3D8R* [15]). All elements adopted a reduced integration scheme. Each shell element was layered and used to represent a group of fabric plies. Typically, three fabric plies having 0/90 or +/-45 fibre orientation directions were considered for each element. Figures 12 shows a detail of the models in the tapered zone. Along the longitudinal and transverse direction an element length of 2 mm was adopted. Symmetry was exploited, whenever possible, to reduce the computational costs.

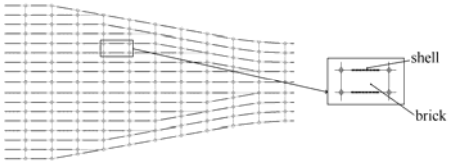

Fig. 12. Detail of the transition zone in the numerical models of the specimens

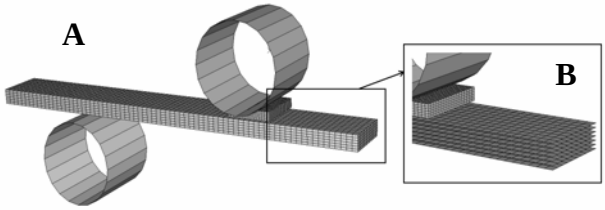

Fig. 13. Model of the reference test (A) and detail of the sublaminates modeled by shells (B)

The cylinders of the test rig were modeled by rigid bodies interacting with the specimen by means of contact algorithms. Moreover the elastomeric pads used in the reference tests were included in the model, using an hyperelastic material law (Fig. 13).

4.2 Calibration and validation of the elastic properties

The available experimental data relevant to the tensile response allowed to determine a preliminary calibration of the material elastic properties. Elastic stiffness in the weft and warp direction of the fabric were considered equal. The out-of-plane elastic stiffness of the interlaminar layers as well as the in-plane compressive stiffness in the reinforcement direction had to be evaluated. Assuming G_{13}=G_{23}, a sensitivity analysis was then performed without activating the damage laws in the material model. The numerical analyses were performed attributing a velocity of 0.3 m/s to the moveable cylinder.

The unique set of parameters identified by this activity obtained a good correlation with the mean average responses of the tests (Fig. 14). To perform the correlation of the reference test,

the compression of the elastomeric pad was subtracted from the time histories of the cylinder displacement both in the experimental as well as in the numerical results.

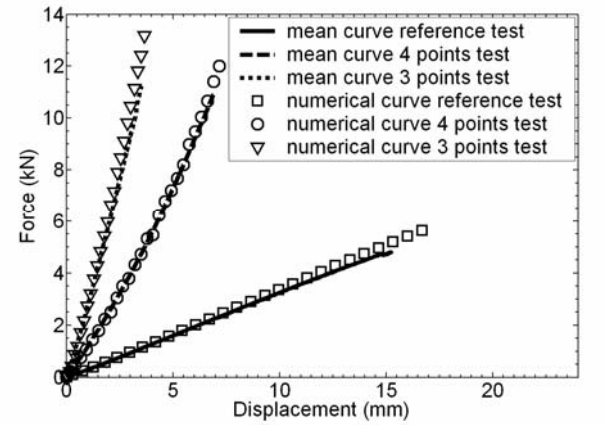

Fig. 14. Numerical-experimental correlation of the force vs. displacement curves

Table 1 reports the in-plane elastic properties derived from the experimental data and from the performed sensitivity analysis. The values of the tensile and compressive elastic moduli were also confirmed by the numerical experimental-correlation of strains on the upper and the lower surface in the reference test.

	E_{11} (GPa)	E_{22} (GPa)	G_{12} (GPa)	ν_{12} (-)	G_{13} (GPa)	E_{33} (GPa)
Tensile	76.0	76.0	4.03	0.07	3.0	7.8
Compressive	68.4	68.4				

Tab. 1. Identified in-plane and out-of-plane stiffness properties of the fabric plies

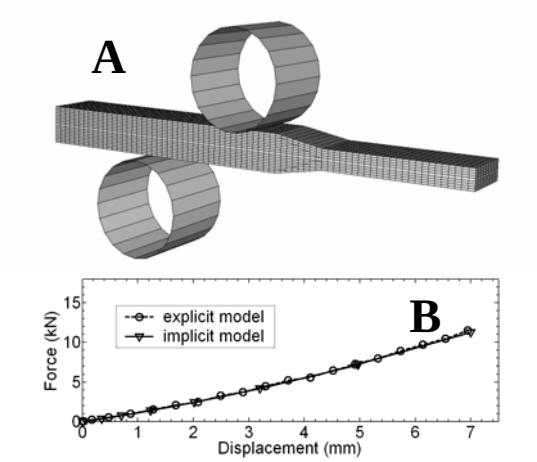

Fig. 15 – HKS/Abaqus Standard model of the four-points bending test (A) and comparison between explicit and implicit analyses (B)

The four-points bending test was also analyzed with a non-linear implicit analysis that was performed with HKS/Abaqus Standard adopting a finite element scheme made of second order elements, with reduced integration (type C3D20R [15]). The material was considered elastic with the same stiffness properties adopted in the explicit computation.

The mesh is shown in Fig 15-A, while Fig. 15-B reports the results of the explicit and the implicit analyses. The comparison proves that inertia forces plays a negligible role in the explicit analyses and confirms that the modeling technique can reliably represent the bending stiffness of a composite laminate.

Explicit analysis, with 64104 d.o.f, took about 10 h CPU on a personal computer with a Pentium IV 3.0 GHz processor, while the non-linear implicit analysis, with 145842 d.o.f., took about 2.5 h.

5 Numerical analyses modelling the inelastic mechanisms in thick composite laminates

The activation of damage laws in the material models allowed to assess the capability of the adopted modeling technique to model the damage and failure modes obtained in the experiments. Damage initiation levels and interlaminar toughness were set to obtain, with a unique set of material parameters, a good numerical-experimental correlation considering the most significant qualitative and the quantitative aspects of the experimental results.

5.1 Identification of damage initiation levels

The fibre damage variables of the in-plane material model described by Eq. 7, were set to represent a brittle failure of the fibre phase at a tensile strain of 12700 με and at a compressive strain of 11130 με, basing on the experimental results. To identify the strength of interlaminar layers, the numerical stress state in the elements close to the zone of interlaminar damage nucleation was analysed in the explicit analyses performed before activating the damage laws.

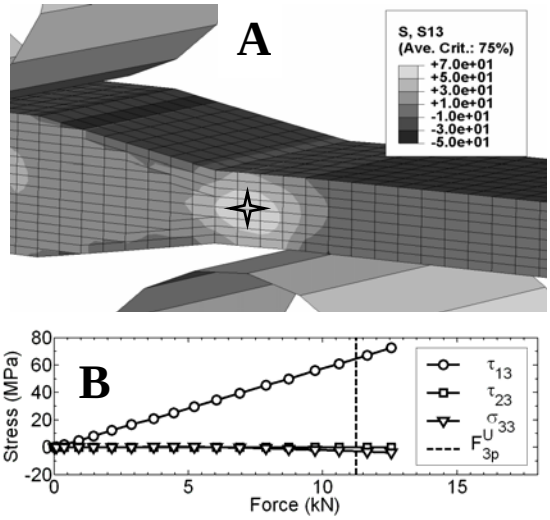

Fig. 16. Contour of stress component σ_{13} in the analysis of the three-points bending test (A) and stress vs. force curves in an element (B)

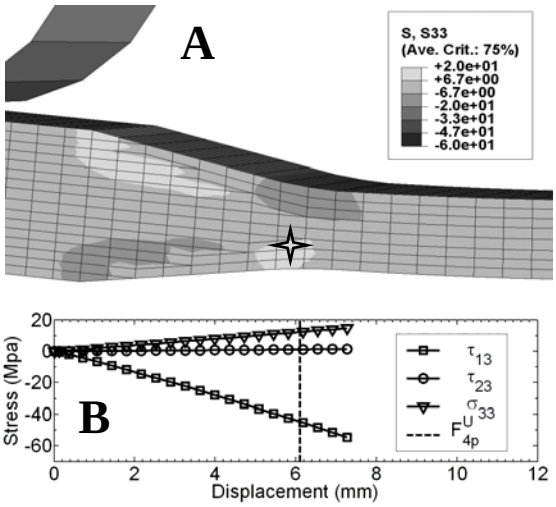

Fig. 17. Contour of stress component σ_{13} in the analysis of the four-points bending test (A) and stress vs. displacement curves in an element (B)

Figure 16-A shows the contour of σ_{13} in the model of the three-points bending test at a load of F_{3p}^{U}. Figure 16-B presents the course of the out-of-plane stress components in a solid element indicated in Fig. 16-A, presenting the maximum values of σ_{13}. Figure 17-A reports the contour of σ_{33} in the model of the four-points bending test, taken at F_{4p}^{P}. According to the analysis, the out-of-plane stress components reach not negligible values in the tapered zone. Particularly, in the lower part of the transition zone, a tensile σ_{33} stress as well as a significant σ_{13} stress component are obtained in the analysis. Figure 17-B shows all the out-of-plane stress components in an element belonging to tapered zone, indicated in Fig. 17-A.

The comparison between the presented numerical results and the experimental failures shows that the models correctly identified the potential locations of interlaminar damage nucleation. Moreover, basing on the quadratic criterion adopted to model the strength of interlaminar layers (Eq. 4), the results presented in Figs. 16,17 allowed to calibrate the strength σ_I^0 and σ_{II}^0 of the interlaminar layers which were set to 17.2 MPa and 64 MPa, respectively.

5.2 Numerical damage evolution and numerical-experimental correlation

The explicit analysis of the three bending tests were performed setting the damage initiation parameters to the previously identified values. The three-points bending test was at first considered to evaluate the behavior of the model at three different levels of interlaminar fracture toughness G_{IIc}, namely 900 J/m^2, 1200 J/m^2 and 1800 J/m^2. A fixed ratio of 0.2 between G_{Ic} and G_{IIc} was maintained. These values were adopted considering the interlaminar properties of unidirectional tapes and fabrics presented in literature [16, 17].

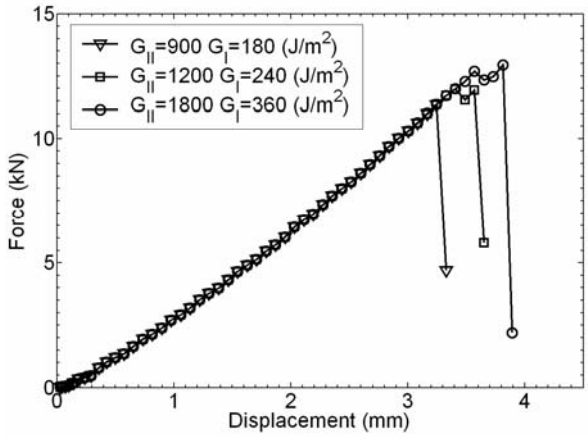

Fig. 18.Sensitivity to G_{IIc} in analysis of the three-points bending test

It can be observed that a variation of G_{IIc} determined a variation of the numerical ultimate load, F_{3p}^{U}, although the damage initiation parameters, σ_{II}^0 and σ_I^0, were kept constant. The

numerical failure mode was characterized by the nucleation of interlaminar damages at the midplane of the specimen, under the cylinder. These damages nucleated and then suddenly propagated in unstable mode in correspondence of the numerical ultimate load carrying capability,. The ratio G_{Ic}/G_{IIc} was varied in the range 0.1 ÷0.3 in order to verify its influence in the development of the minor interlaminar damages and in the propagation of the midplane cracks. The result obtained with G_{IIc}=1200 J/m^2 and G_{Ic}/G_{IIc} = 0.1 presents a development of interlaminar damages close to the experimental results (Fig. 19). However, in the numerical computations, damages always propagated instantaneously without developing by subsequent steps of unstable propagation as in the experiments. The analyses of the four-points bending test were performed with material properties presented in Tab. 2.

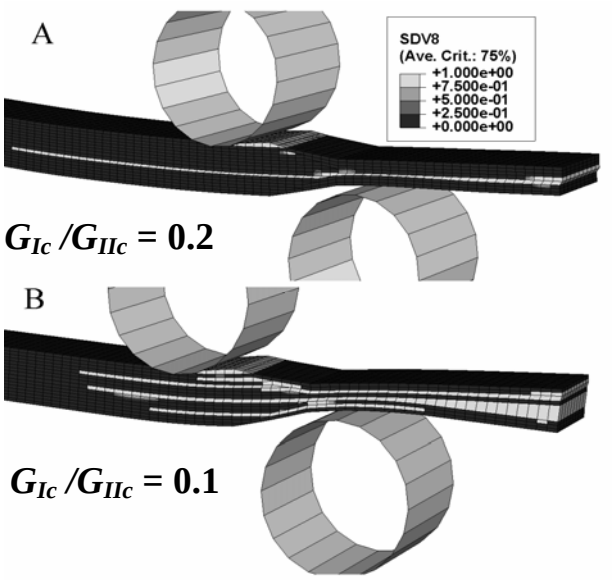

Fig. 19. Damages in the analyses of the three-points bending test using G_{IIc}=1200 J/m^2

σ_I^0 (MPa)	σ_{II}^0 (MPa)	G_{Ic} (J/m^2)	G_{IIc} (J/m^2)
17.2	64.0	120	1200

Tab. 2. Interlaminar layer properties used in the analysis of the four-points bending test

Figures 20-A,B show, respectively, the nucleation and the propagation of the interlaminar damage in the analyses of the four-points bending test, while Fig. 20-C refers to the ultimate compressive failure.

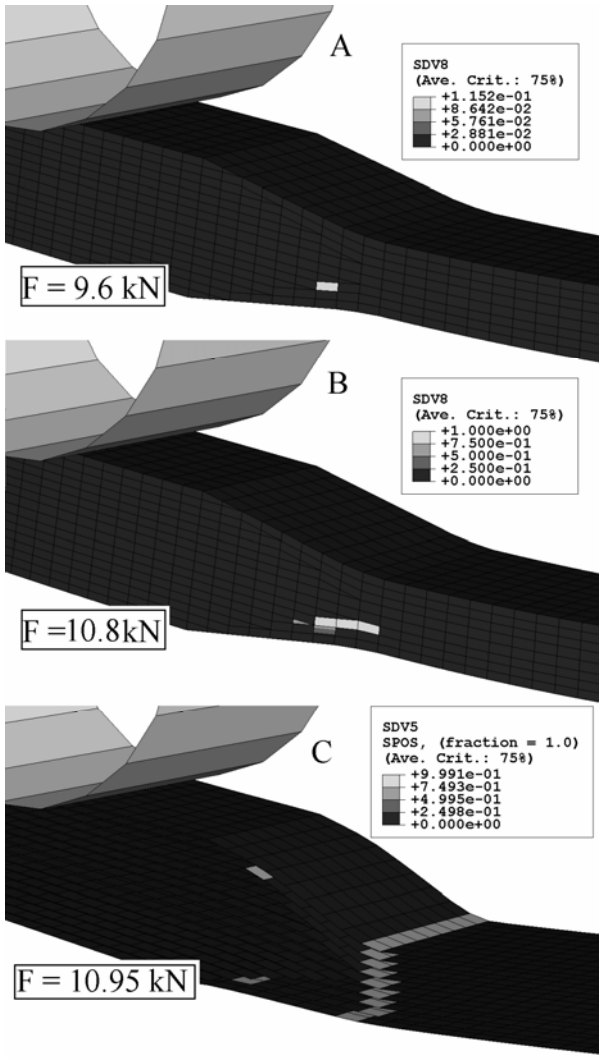

Fig. 20. Nucleation and propagation of the crack in the analysis of the four-points bending test

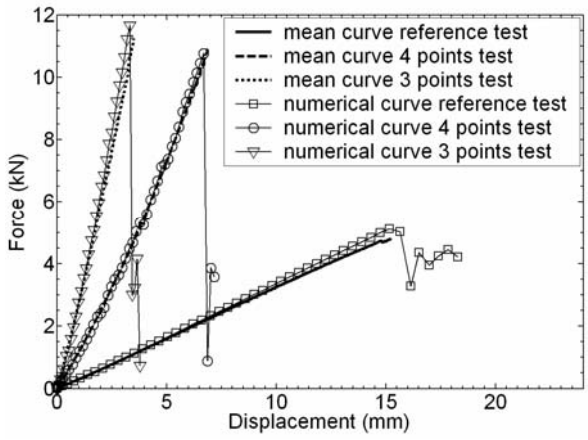

Fig. 21. Numerical-experimental correlation of the force vs. displacement curves

Finally the complete numerical-experimental correlation is presented in Fig. 21, showing that also the prediction of the numerical load at failures is in appreciable agreement with the experimental data.

6 Conclusions

The performed bending experiments on thick composite laminates obtained damage and failure modes significantly influenced by the out-of-plane stress components acting in the interlaminar layers. The adopted modeling technique allowed to model the interlaminar layers between sublaminates in the specimens at a still acceptable computational cost. An interface constitutive law has been applied within the chosen modeling strategy. The numerical approach was used to identify the most significant material parameters influencing the response of the specimens and correctly represented the bending stiffness of thick composite laminates in various conditions. The calibrated models, developed without any assumption on the zones of potential damage nucleation, obtained also a good numerical-experimental correlation considering the failure modes, the zone of nucleation and the propagation mode of interlaminar damages as well as the ultimate load carrying capability of the specimens in all the considered tests.

References

[1] Corigliano A, Formulation, identification and use of interface models in the numerical analysis of composite delamination, *Int. J. Solids and Structures*, Vol. 30, 1993, pp. 2779-2811.

[2] Hilleborg A, Modeer M, Paterson P E, Analysis of crack formation and crack growth in concrete by fracture mechanics and finite elements, *Cement and Concrete Research*, Vol. 6, 1976, pp. 773-782.

[3] Mi Y, Criesfield M A, Davies G A., Hellweg H B, Progressive delamination using interface elements, *Journal of Composite Materials*, Vol. 32, No. 14, 1998, pp. 1246-1272.

[4] Reedy E. D Jr, Mello F J, Guess T R, Modelling the initiation and growth of delaminations in composite structures, *Journal of Composite Materials*, Vol. 31, No. 8, 1997, pp. 812-831.

[5] De Moura M, Goncalves, J, Marqus, A., de Castro P, Modeling compression failure after low velocity impact on laminated composite materials using interface elements, *Journal of Composite Materials*, Vol. 31, 1997, pp. 1462-1479.

[6] Wisheart M, Richardson M, "The finite element analysis of impact induced delamination in composite materials using a novel interface element", *Composite Part A*, Vol. 29A, 1998, 301-303.

[7] Davila C, Mixed mode dechoesion elements for analyses of progressive delaminations, *42nd AIAA/ASME/ASCII/AHS/ASC Structures, Structural Dynamics, and Materials Conference and Exhibit*, , Seattle, WA, U.S.A., 16-19 April 2001.

[8] Airoldi A, Sala G, Modeling of composite interlaminar damage in explicit FE codes, *XVII Congresso Nazionale AIDAA*, Roma, Italy, 15-19 Sept. 2003.

[9] Philips E, Herakovich C., Gragam L., Damage development in composite with large stress gradients, *Composite Science and Technology*, Vol. 61, pp. 2169-2182, 2001

[10] Bianchi S., Corigliano A., Frassine R., Rink M., Modelling of interlaminar fracture processes in composite using interface elements, *Composite Science and Technology*, Vol. 66, pp. 255-263, 2006

[11] Johnson A, Holzpapfel M., Modeling of soft body impact on composite structures, *Composite Structures*, Vol . 61, pp. 103-113

[12] Airoldi A., A constitutive law for progressive damage in composite materials, PhD Thesis, Politecnico di Milano, Dip. Ing. Aerospaziale, 2002

[13] Airoldi A, Lanzi L, Sala G, Shear post-buckling behavior of Glare modeling fiberglass damage, *47th AIAA/ASME/ASCII/AHS/ASC Structures, Structural Dynamics, and Materials Conference and Exhibit*, , Newport, RI, USA, 1-4 May, 2006.

[14] Airoldi A., Sala G., Experimental investigation and numerical modeling of Glare inelastic behaviour, XVIII Congresso Nazionale AIDAA, Volterra, Italy, 19-22 Sept. 2005

[15] *Abaqus® Theory and User's Manuals*, Hibbit, Karlsson & Sorensen, Pawtucket, USA, 1998

[16] Carlsson, L. ., Gillespie, J. W., Mode-II interlaminar fracture of composites, in *Application of the fracture mechanics to composite materials*, Editor Friedrich, K., Composite Material Series No. 6, Elsevier Science Publishers B.V., 1989

[17] Wang Y., Zhao D., Characterisation of interlaminar fracture behavior of woven fabric reinforced polymeric composites, *Composites*, Vol. 26, pp. 115-124, 1995.